

Roof tile frangibility and puncture of metal window shutters

Sylvia T. Laboy-Rodriguez, Daniel Smith, Kurtis R. Gurley* and
Forrest J. Masters

Department of Civil and Coastal Engineering, University of Florida, USA

(Received May 4, 2012, Revised October 4, 2012, Accepted October 21, 2012)

Abstract. The goal of this study was to investigate the vulnerability of roof tile systems and metal shutters to roof tile debris. Three phases addressed the performance of tile roof systems and metal shutters impacted by roof tile debris. The first phase experimentally evaluated the tile fragment size and quantity generated by a tile striking a tile roof system. The second phase experimentally quantified the puncture vulnerability of common metal panel shutter systems as a function of tile fragment impact speed. The third phase provided context for interpretation of the experimental results through the use of a tile trajectory model. The results provide supporting evidence that while metal panel window shutters provide significant protection against a prevalent form of windborne debris, these systems are vulnerable to tile fragment puncture in design level tropical cyclones. These findings correlate with field observations made after Hurricane Charley (2004).

Keywords: windborne debris; missile impact; roof tiles; window shutters; puncture

1. Introduction

Post-storm investigations have demonstrated that windborne debris can cause significant damage to the building envelope (Meloy *et al.* 2007) and that window protection can be an effective mitigation measure (Gurley and Masters 2011). This report discusses the third in a series of investigations regarding the vulnerability of windows and window protection systems to windborne debris. The two previous studies addressed the vulnerability of unprotected residential window glass to impact from roof shingles and small vegetation (Masters *et al.* 2010), and the performance of metal shutters under impact by full roof tiles (Fernandez *et al.* 2010).

The current study addresses the frangibility of roof tile systems under impact by roof tiles, and the vulnerability of metal shutters under impact by roof tile fragments. The distribution of tile fragment sizes (ratio of tile fragment weight to full tile weight) produced when a tile roof system is impacted by a roof tile, and the speed and momentum thresholds that lead to metal shutter puncture by tile fragments were quantified experimentally. Additionally, a numerical study of tile fragment trajectories was conducted to quantify the speed of tile fragment impact on fenestration. Variables included mean wind speed, tile fragment size (by weight), turbulence intensity, and the distance between fragment source and impacted fenestration. The results from these three phases

*Corresponding author, Associate Professor, E-mail: kgurl@ce.ufl.edu

were combined to provide an assessment of the risk of metal shutters to puncture from tile fragments as a function of tropical cyclone severity.



Fig. 1 Tile Debris Damage after Hurricane Charley, Punta Gorda, FL 2004, Left: Map of Punta Gorda, FL (Courtesy of Google Maps), Center and Right: Tile Debris Damage in Punta Gorda, FL

2. Background

Windborne debris is a large contributor to building envelope damage during windstorm events. This problem can be defined in terms of the windborne debris load (types and sources of debris, trajectory and speed) and the vulnerability of building components to the windborne debris impacts. The literature addresses the former problem in numerous studies of windborne debris trajectories via numerical modeling and experiments. The subject of component capacity has largely focused on glass damage and the development of impact standards for protective devices. The current study addresses both aspects of the problem within the context of roof tile fragments impacting metal shutters.

Several researchers have conducted studies to document vulnerability and quantify the risk of damage to fenestration (e.g., Beason 1974, Minor 1994, 2005, Masters *et al.* 2010, Fernandez *et al.* 2010, Lin and Vanmarcke 2008, 2010a, b, Yau Siu *et al.* 2011). Masters *et al.* (2010) identified the momentum threshold required to damage unprotected residential glazing impacted by asphalt shingles and small vegetation representing tree branches. In a follow up study, the deformation of metal shutters under impact by a full 4.1 kg roof tile and 4.1 kg 2x4 lumber (as per ASTM) was quantified (Fernandez *et al.* 2010). The deformations caused by the tile impact typically exceeded the installed distance from the glass (setback) required for the tested product. Shutter puncture was not observed in these experiments, but this is known to occur from post-tropical cyclone field studies. This prompted the current study of tile fragment impact on these same metal shutter products.

During the 2004 Atlantic hurricane season, field observations demonstrated that roof tile windborne debris caused severe damage to the building envelope. Fig. 1 shows two examples of such damage in Punta Gorda, Florida after Hurricane Charley. Tile debris was identified to be a significant source of windborne debris in this region (Meloy *et al.* 2007).

Many researchers have conducted experiments and developed models to predict the trajectory of windborne debris. Tachikawa (1983, 1988) conducted experiments to measure the trajectory of debris in a wind tunnel and compared the results with the numerical solutions by applying the two dimensional equations of motion for square and rectangular flat plates in uniform flow. Wills *et al.* (2002) modeled and validated a flight initiation condition. Wang (2003) conducted wind tunnel tests to investigate flight initiation speed and behavior for sheet debris. Holmes and Mullins (2001) presented an analysis that estimates the distance and travel time of debris. Holmes (2004) studied the trajectories of spheres in severe storm weather considering the effect of turbulence in the wind velocities. Lin *et al.* (2006) conducted wind tunnel and full scale experiments to investigate the trajectory, and velocity of plate type debris. Holmes *et al.* (2006) developed a numerical model of a square plate and presented a comparison of the results with the experimental data obtained from Tachikawa. Baker (2007) presented equations of motion for sheet and compact objects, and presented a comparison of the numerical solutions with experimental results of Tachikawa (1983) and Wills *et al.* (2002). Visscher and Kopp (2007) studied the flight mechanics for a plate initially mounted on a roof of a 1:20 scale model to determine the motion type and the trajectory. Following this study, Kordi *et al.* (2010) conducted experiments to analyze the flight of sheathing panels subjected to different wind directions. Kordi and Kopp (2009a) performed an analysis of windborne plates based on the quasi-steady model and compared the numerical solution with the experimental results from Tachikawa (1983) and Lin *et al.* (2006). Scarabino and Giacopinelli (2010) conducted a dynamic analysis on the 2D equations for sheet debris by comparing aerodynamic coefficients of two models. Richards *et al.* (2008) presented a 3D model of the trajectory of windborne debris.

3. Methodology and results

This section presents the methodology and results for the three study phases. Phase 1 experimentally quantified the statistical distribution of tile fragment sizes (ratio of tile fragment weight to full tile weight) produced when a tile roof system is impacted by a tile. Phase 2 experimentally quantified the probability of metal shutter puncture when impacted by a tile fragment. Phase 3 numerically evaluated the velocity of a tile fragment impacting the roof and windows of a house through the use of a trajectory model and coefficients adopted from the literature (Tachikawa 1983,1988, Holmes 2004, Holmes *et al.* 2006, Baker 2007, Lin *et al.* 2007, Kordi and Kopp 2009b). The outcomes of the three phases were combined to provide an assessment of the risk of tile fragments puncturing shutters as a function of wind conditions.

3.1 Phase 1: tile fragility

Phase 1 was designed to produce a statistical assessment of the size of tile fragments produced when a tile roof system is impacted by a tile or tile fragment from a neighboring house. The influence of tile installation (mechanical or mortar set), and speed and weight of the impacting tile were considered.

A series of roof structures were constructed. Tile roof cover was installed by a licensed roofing contractor (Fig. 2). These roof systems were then subjected to impact by tiles using an apparatus that allows precise control of impact location and speed. The test matrix consists of 24 combinations of the following variables:

- Two shapes of concrete tile
- Mortar set or mechanical fastening (single screw)
- Impacting tile: half size (by weight) and whole tile
- 3 impact speeds (15.2, 22.4, 29.5 m/s)

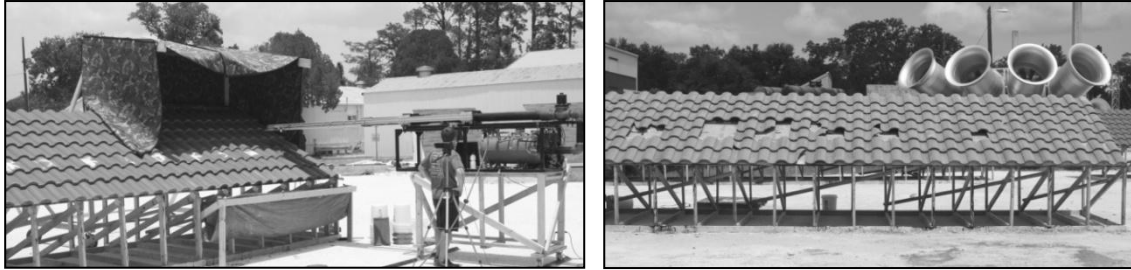


Fig. 2 Images of phase 1 frangibility testing, Left: Set up for tile frangibility impact test prior to tile launch (phase 1 testing), Right: Roof system post-impact testing

3.1.1 Tile launching apparatus

The tile launching apparatus is comprised of four components; the pneumatic ram that propels the tile along a track toward the target, the air reservoir and barrel that supply propulsion force to the ram, the electronic valve that releases the pressure from the tank to the barrel, and the integrated electronic system.

Fig. 3 presents an illustration of the launching apparatus. The air reservoir is coupled to a steel pipe connected to an electronic valve. The ram fits within the barrel and harnesses the released pressure. The far end of the ram bears against the tile projectile. A launch deck extends from the exit of the barrel toward the target. The tile projectile sits upon this deck and is propelled toward the target via the ram. The electronic system includes feedback control for filling, purging and maintaining air reservoir pressure, control of the electronic valve for launch, and measurement of the projectile speed using photoelectric sensors. This system is controlled from a custom National Instruments LabVIEW application.

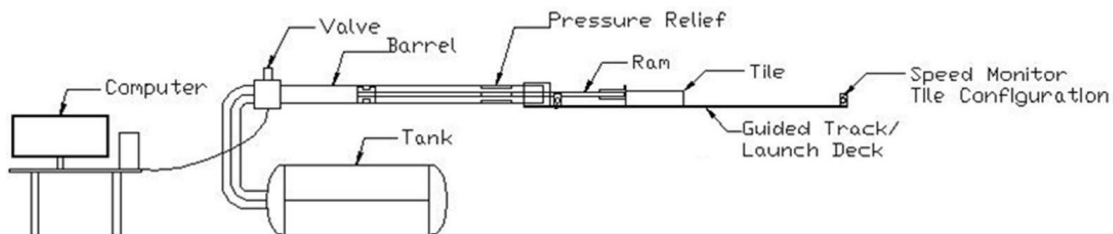


Fig. 3 Tile launch apparatus (phase 1 and phase 2 testing)

3.1.2 Tile projectile impact angle and speeds

Concrete roof field tiles were impacted with half and full size concrete tiles. The impact angle is horizontal in all cases. Tests were conducted at speeds of 15.2, 22.4 and 29.5 m/s. Speed was calibrated to the launch air pressure using a high speed camera and photoelectric sensors to monitor the speed of the projectile as it left the launcher.

Table 1 Summary results of Phase 1 tile fragility testing

Tile Material	Size	Attachment	Cell Content:		
			Mean (standard deviation) [# of fragments]		
			Decimal values are a fraction of full tile by mass		
			15.2 m/s	22.4 m/s	29.5 m/s
Concrete I	Full	Mortar	0.034 (0.008) [3]	0.086 (0.090) [15]	0.087 (0.098) [23]
	Full	Mechanical	0.109 (0.148) [66]	0.146 (0.165) [48]	0.119 (0.189) [110]
	Half	Mortar	0.075 (0.078) [3]	0.042 (0.011) [3]	0.137 (0.155) [13]
	Half	Mechanical	0.097 (0.123) [24]	0.092 (0.132) [37]	0.105 (0.158) [42]
Concrete II	Full	Mortar	0.108 (0.194) [9]	0.094 (0.074) [31]	0.129 (0.167) [71]
	Full	Mechanical	0.130 (0.192) [70]	0.125 (0.149) [61]	0.121 (0.163) [110]
	Half	Mortar	0.123 (0.058) [3]	0.082 (0.103) [15]	0.108 (0.122) [28]
	Half	Mechanical	0.085 (0.062) [4]	0.122 (0.131) [24]	0.145 (0.171) [48]

3.1.3 Results of phase 1: tile fragility tests

Each of the 24 test combinations was repeated three times and the results combined to produce Table 1. Concrete I are classic Spanish design high profile field tiles and weigh approximately 4500 grams. Concrete II are S-shaped high profile field tiles and weight approximately 4100 grams. Upon impact, the fragments from the impacted tiles and impacting tile were separated via color (the impacting tile was painted) and each fragment individually weighed and dimensioned. Many fragments were not much larger than small gravel, and were deemed too small to pose a threat of metal shutter puncture. Thus fragments with less than 2% of the full tile weight were discarded from the analysis and all discussion hereafter. Only fragments from the impacted tiles are included in Table 1. Each cell in the table contains three values: the mean size of the tile fragment (defined as the ratio of the fragment weight to full tile weight), the standard deviation of same (in parentheses), and the total number of fragments (larger than 2% of the full tile by weight) produced from the three tests [in brackets].

The value of this analysis lies in the relative statistics among the combinations (trends relative to test conditions). For example, tiles that were attached via mortar produced fewer fragments than the mechanically attached tiles. Fig. 4 (right) shows the tile fragments produced from the 15.2 m/s test of a full tile impacting a mechanically fastened roof tile system. The trends that emerge from the analysis are:

- The mean value of the fragment size is approximately $1/8^{\text{th}}$ of the full tile by weight. Lower mean values in Table 1 are associated with cases with very few fragments.
- Higher impact speeds produced more fragments, but the mean size of these fragments did not change significantly.
- Full tile debris produced more fragments than half tile debris, but the mean size of these fragments did not change significantly.
- Mechanically attached (single screw) roof systems produced more tile fragments than mortar set roof systems, all other variables being equal.
- The mean size and number of fragments did not change significantly between the two tile shapes (Concrete I or II).
- The probabilistic distribution of tile fragment sizes is closely modeled by an exponential distribution (not shown).

Phase 1 results justified the tile fragment shapes and sizes used for the phase 2 experimental testing to evaluate the vulnerability of metal shutters to tile fragment puncture. In phase 2, $1/8^{\text{th}}$ and $1/4^{\text{th}}$ tile fragments (by weight) were used. The results from the phase 1 study did not include tile roof debris produced by wind uplift.

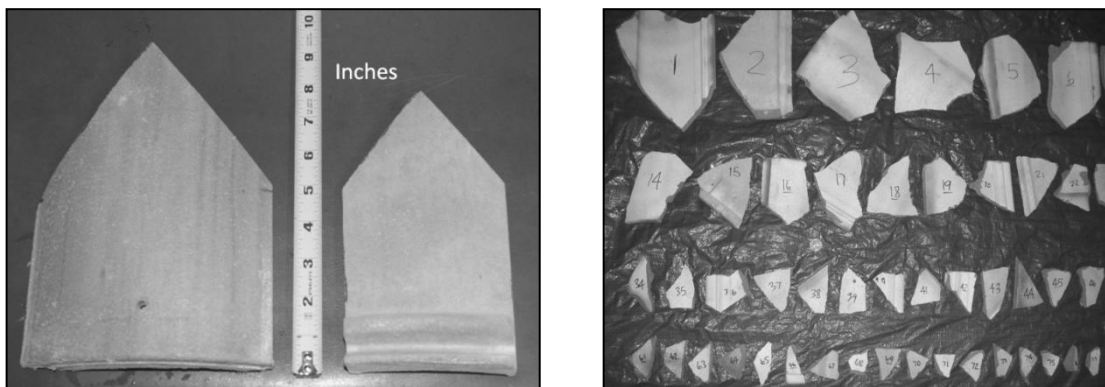


Fig. 4 Images from phase 2 and phase 1 testing, Left: $1/4^{\text{th}}$ and $1/8^{\text{th}}$ size (by weight of a full tile) tile fragments used as the impact debris for phase 2, Right: A sample of roof system tile fragments produced from phase 1 testing

3.2 Phase 2: shutter puncture vulnerability

Phase 2 investigated the vulnerability of metal shutters to puncture from roof tile debris. The probability of shutter puncture was quantified as a function of debris size, speed and momentum in the form of empirical vulnerability curves.

Tile fragments were launched toward properly installed (according to manufacturer specifications) metal shutters with a controlled speed, impact location and impact orientation. Twenty tests were conducted for any given set of control variables. The test matrix consists of the following variables:

- Tile fragment size ($1/8^{\text{th}}$ and $1/4^{\text{th}}$ of a full tile by weight)

- Impact speed (ranging from 21 m/s to 37 m/s)
- Metal shutter material (aluminum or steel)
- Metal shutter thickness (aluminum – 1.27 mm and 1.56 mm, steel – 22 gage and 24 gage)

3.2.1 Tile launching apparatus

The tile launching apparatus is discussed in the previous section and shown in Fig. 3. Photoelectric sensors documented the launch speed of every test. The end of the launch deck, where the photoelectric sensor was located, was less than 10 feet from the shutter.

3.2.2 Tile fragment projectile

Impact testing was conducted using concrete tile fragments $1/4^{\text{th}}$ and $1/8^{\text{th}}$ of a full size concrete tile by weight. These fragments were cut from a full tile using identical dimensions for every fragment of a given size. Fig. 4 (left) shows the two fragment sizes used. Tile fragments from the phase 1 tile fragility testing (Fig. 4 right) demonstrated that ‘pointy’ fragments were commonly produced. Impact orientation was always point first and perpendicular to the shutter plane. This is a conservative approach that will produce the low end of the range of puncture speeds under field conditions. A new fragment was used for every test.

3.2.3 Shutters tested

Steel shutters of two thicknesses (22 and 24 gage) and aluminum shutters of two thicknesses (1.27 and 1.56 mm, referred to as 050 and 060 respectively) were tested. All products are approved for use in Florida. Panels ranged between 330 and 378 mm wide and each was 1.68 m tall. Three overlapping panels were direct mount installed in a vertical orientation, bearing against the frame at the top and bottom with no bearing along the vertical edges. The wood frame has studs installed at 152 mm on center or 159 mm on center across the top and bottom horizontal framing borders. The panels were fastened by a wing nut on each stud. A 1.70 m high and 1.52 m wide wood frame bolted to a strong floor supports the storm panels during testing. The dimensions of the frame opening are 1.60 m wide by 1.57 m high.

3.2.4 Puncture definition

The test conditions resulted in either deformation only, or deformation with tearing. The tile fragment shown in Fig. 5 (upper right) was used to define puncture. If this fragment passed through the tear, the result was defined as a puncture (Fig. 5 lower right). If this fragment could not pass through the tear, the result was not a puncture (Fig. 5 lower left). Only punctures are considered a failed state.

3.2.5 Test protocol

The probability of failure for a given shutter type impacted by a given tile fragment was evaluated at a given speed by subjecting the shutter type to 20 identical impact tests. Each test targeted a corner of the panel system that had not been impacted (repeat impacts were not considered). The impact location was within 200 mm of the corner of a shutter panel (Fig. 5, upper left). The puncture probability is the number of punctures divided by 20. The series of 20 tests is conducted for at least three speeds for a given shutter type and fragment size.

The speed of every impact was recorded via photoelectric sensors located at the end of the guided track (Fig. 3). The highest coefficient of variation (COV) among the impact speeds for any

set of 20 tests was less than 0.08 (worst case), and the average COV was less than 0.04. Results reference the mean impact speed among the 20 tests.

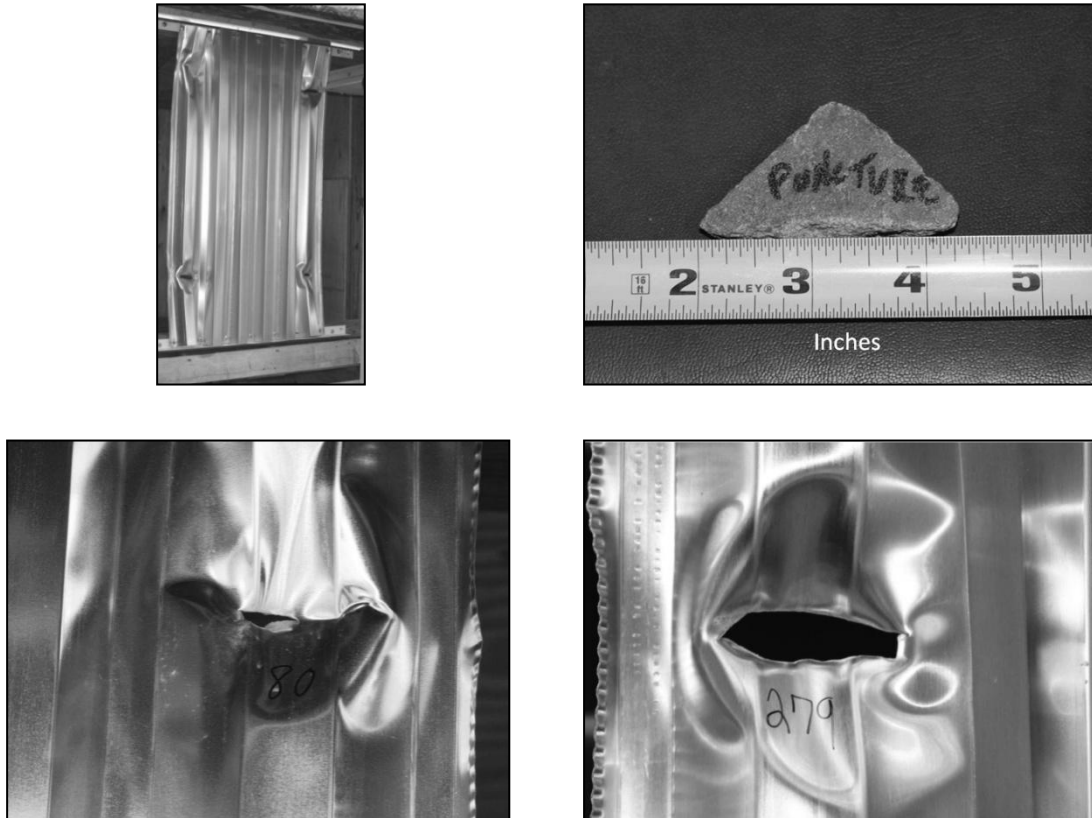


Fig. 5 Images from phase 2 shutter puncture testing, Upper left: Installed three panel shutter system after four impact tests, Upper right: Tile fragment used to define puncture, Lower left: An example of a tear but not puncture, Lower right: An example of a puncture

3.2.6 Results of phase 2: shutter puncture vulnerability tests

Fig. 6 presents the puncture probability results. Consider the diamond within a large circle in the bottom right plot in Fig. 6. This data point corresponds to the 22 gage steel product, and was produced from the result of 20 1/4th size concrete tile fragment impacts at the same impact speed of 34 m/s (coefficient of variation less than 0.05). In this case, 16 of the 20 tests resulted in puncture (0.8 vertical axis).

Each of the data points in Fig. 6 has an associated uncertainty based upon the use of 20 individual impacts to generate a given value. The 95% confidence interval for each data point is plus or minus 0.2 on the vertical axis. That is, if a given test sequence of 20 specimens was repeated many times, the confidence interval represents the range in which the probability of puncture results are expected to fall for 95% of these sequences. The confidence intervals were calculated assuming that the outcome from any 20 specimens is binomially distributed. This

requires that any one test has two possible outcomes (puncture or non-puncture) and that each test is not influenced by any previous test. Both of these conditions are met by the test protocol. The 95% confidence interval was validated using a Monte Carlo simulation.

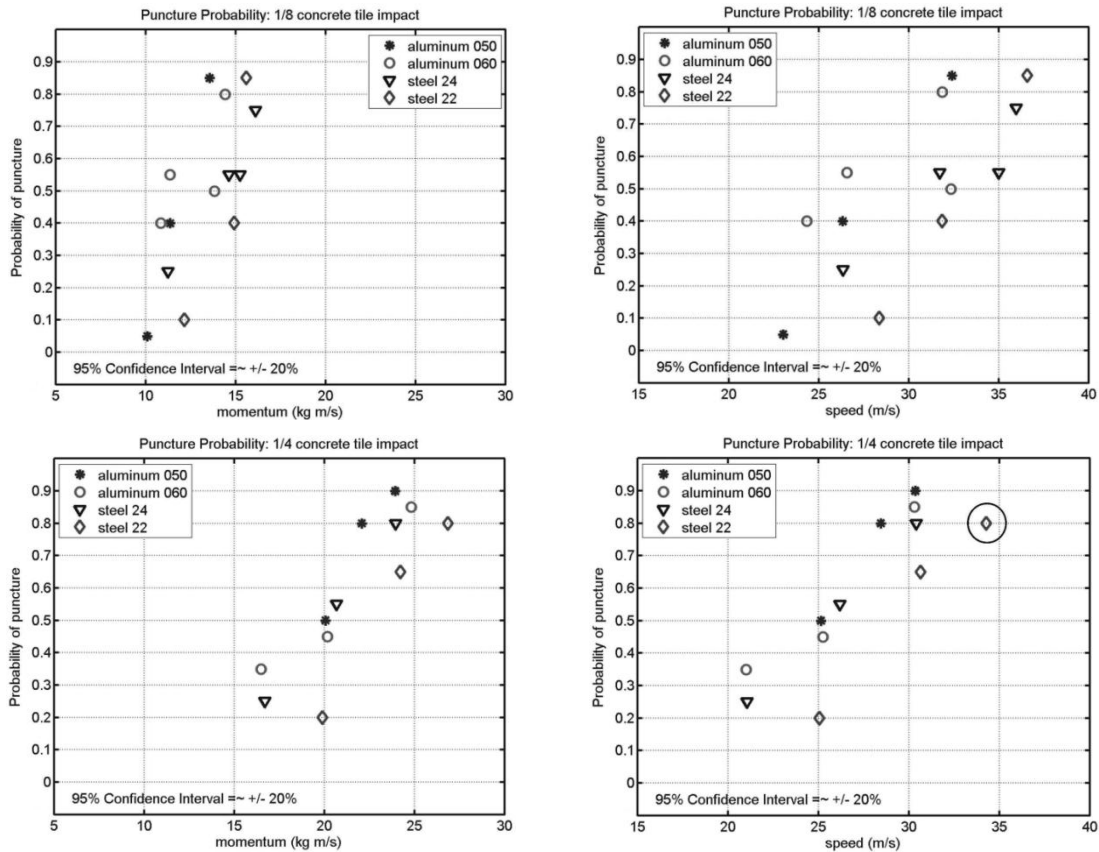


Fig. 6 Puncture vulnerability curves for 1/8th and 1/4th tile fragment impacts as a function of impact momentum (1/8th – left upper, 1/4th – left lower) and impact speed (1/8th – right upper, 1/4th – right lower). The 95% confidence interval refers to the vertical axis. The circled diamond is referred to within the text.

Results show that the speed associated with a given probability of puncture is higher for the 1/8th tile than the 1/4th tile, and that the thickest steel (22 gage) provides the highest resistance to puncture, as expected. For the 1/8th tile fragment, puncture becomes possible at impact speeds approaching 25 m/s, and exceed 50% likelihood at approximately 30 m/s. Beyond 35 m/s all products tested in this study are likely to experience puncture upon impact.

The impact speed of the tile fragment is related to the speed and turbulence characteristics of the wind carrying the tile fragment. The trajectory model study will provide relationships between the tile fragment impact speed and the speed of the wind carrying the fragment (referenced to 3 second open exposure isotachs from ASCE 7), the turbulence intensity, the size of the fragment,

and the distance traveled from debris source to shutter. The discussion of likelihood of puncture will be recast in terms of tropical cyclone intensity upon presentation of the trajectory model.

3.3 Phase 3: trajectory model

Phase 2 determined the puncture vulnerability thresholds for shutter products impacted by roof tile fragments. The purpose of the trajectory model is to determine the velocity of tile fragment impact on the roofs and shuttered windows on structures that are in close proximity to the source of the fragments (the target is a neighboring house across the street). The combined outputs of the experimental and modeling phases will project the tropical cyclone conditions in which metal shutter puncture becomes a possible scenario.

The trajectory model tracks the flight of a tile fragment that is released from rest on a sloped roof. The variables in this experiment include:

- Tile fragment size (1/8th and 1/4th of full tile by weight)
- Distance from tile source to target house (from 30 m to 60 m)
- Reference wind speed carrying the fragment: Open exposure 3 second gust values of 44.72 m/s to 89.44 m/s in 4.47 m/s increments (referenced to the wind speed isotachs in ASCE 7 (ASCE 2010))
- Reference turbulence: Exposures D, C and B in ASCE 7 (ASCE 2010)

The trajectory of the fragment includes its position in space, orientation, and speed. Any given trajectory is calculated in time increments of 0.02 s throughout the duration of flight. This time stepping spatial position is used to determine speed upon impact. The tile fragment size, mass, distance to target, reference wind speed and reference turbulence are fixed for a given trajectory experiment.

A Monte Carlo simulation methodology was employed. 100,000 trajectory experiments were conducted for a given fragment size, distance to target, reference wind speed and reference turbulence. The horizontal wind speed acting on the tile fragment was based on the reference wind speed and turbulence, and is a random quantity. Any one trajectory experiment utilized a new randomized trace of instantaneous horizontal wind speed, providing a unique trajectory. These thousands of trajectories were used to project the probability of the fragment impacting the neighboring roof or fenestration across the street, and the fragment speed associated with that impact.

3.3.1 Calculation of wind speed traces

Wind speed traces were calculated for 11 ASCE 7 (ASCE 2010) isotachs from 44.72 m/s to 89.44 m/s in increments of 4.47 m/s. Each 3-second, exposure C, 10 m height isotach was converted to an hourly mean wind speed for exposures B, C, and D for a total of eleven mean wind speeds per exposure via

$$\bar{U} = \hat{u}_{3sec exp C} * \frac{\sqrt{k_z}}{GF} \quad (1)$$

where $\hat{u}_{3sec exp C}$ is the 3-second gust wind speed, k_z is the velocity pressure exposure coefficient (table 27.3-1 ASCE 10), GF is the gust factor for exposures B, C, and D (values are 1.71, 1.53, 1.42, respectively).

The power spectrum of the fluctuating wind for each hourly mean velocity and exposure was assigned the form proposed by von Karman (1948) for homogeneous isotropic turbulence for strong winds in a neutral atmosphere

$$\frac{nS_u(n)}{\sigma^2 u} = \frac{4\tilde{n}}{(1 + 70.8\tilde{n}^{2^{5/6}})} \quad (2)$$

where $\tilde{n} = \frac{nL_{ux}}{\bar{U}}$, n is the frequency, $\sigma^2 u$ is the variance of the wind velocity, and L_{ux} is the horizontal integral length scale which is a function of the terrain roughness

$$L_{ux} = l\left(\frac{\bar{z}}{10}\right)^{\bar{\epsilon}} \quad (3)$$

where l is the integral length scale (ASCE 7-10 Table 26.9-1), \bar{z} is the height of the structure, and $\bar{\epsilon}$ is the integral length scale power law exponent (ASCE 7-10 Table 26.9-1). This spectral model is a function of both mean wind speed and exposure. Thus 33 power spectra (11 isotachs for exposures B, C, D) were standardized and applied to generate 1 hr Gaussian signals using a random amplitude and random phase technique in the frequency domain (Shinozuka and Deodatis 1991).

This spectral model is for horizontal turbulence relative to a fixed point in the atmosphere. This simplified approach does not model the effect of vertical turbulence or a frame of reference that travels with the object. The inclusion of a moving perspective introduces a non-stationary aspect to the simulation which, following Holmes (2004), was deemed unnecessary for objects with short flight times and speeds that are a fraction of the wind speed carrying them. Initial experiments indicated that the tile fragment debris trajectories had flight times of one or two seconds, which conforms to previous study findings (e.g., Holmes 2004, Lin *et al.* 2006, Holmes *et al.* 2006).

Holmes (2004) also noted a slight underestimation of horizontal velocity of the object when ignoring vertical turbulence. In the current study this is offset in part by an overestimate of horizontal velocity via use of a 2D model (discussed in section 3.3.4).

In order to be conservative in the trajectory analysis, the highest 5 s segment from each simulated hour was isolated using a moving average. Then each five second signal was scaled and dilated to obtain an instantaneous horizontal wind speed trace (to be used as input to the trajectory model) as follows

$$u = u' + \bar{U} \quad (4)$$

where u' is the component in the direction of the mean wind due to the turbulence (highest 5 s segment from the hour), and \bar{U} is the hourly mean wind speed at 10 m (Table 2). The standard deviation (σ_u) was determined from the modified Harris and Deaves equation (1981)

$$\sigma_u = \frac{u_* 7.5\eta \left[0.538 + 0.09 \ln \left(\frac{\bar{z}}{z_0} \right) \right]^{\eta^{16}}}{1 + 0.156 \ln \left(\frac{u_*}{fz_0} \right)} \quad (5)$$

The shear velocity u_* was calculated using the logarithmic law $u_* = \frac{\bar{U} * k}{\ln(\frac{z}{z_0})}$, where k is the von Karman constant (0.40), z_0 is the roughness length (0.20, 0.02 and 0.005 for B, C and D from Table 27.3.1 ASCE 7-10, $\eta = 1 - \frac{6fz}{u_*}$, $f = 2 * \omega * \sin(\lambda)$ (Coriolis force), $\omega =$ earth rotation speed = $7.29 * 10^{-5}$ (rad/sec), and λ is latitude (25° is used for Florida). The application of Harris and Deaves and the hourly mean wind speeds in Table 2 produce turbulence intensities of 0.240, 0.185 and 0.168 for exposures B, C and D, respectively at 10 m.

3.3.2 Calculation of the debris trajectory

It was assumed that any loose fragments on the source roof will become airborne following the criteria of Wills *et al.* (2002) and Holmes (2007). Once airborne, the motion of the fragment was calculated following a trajectory model and aerodynamic coefficients adopted from the literature (Tachikawa 1983, 1988), Holmes (2004), Holmes *et al.* (2006), Baker (2007), Lin *et al.* (2007), Kordi and Kopp (2009b)). The initial vertical position was assumed to be 8.54 m as the height at the ridge of a two story house.

Table 2 3-second gust exposure C isotach reference and hourly-mean wind speeds

3-sec gust isotach (m/s)	Hourly Mean Wind Speeds (m/s)		
	Exposure B	Exposure C	Exposure D
44.72	22.14	29.20	34.17
49.20	24.38	32.16	37.57
53.67	26.57	35.06	41.01
58.14	28.80	37.97	44.41
62.62	30.99	40.92	47.85
67.08	33.23	43.83	51.25
71.56	35.47	46.74	54.65
76.03	37.66	49.69	58.09
80.50	39.89	52.60	61.49
84.97	42.08	55.50	64.94
89.45	44.32	58.45	68.34

3.3.3 Probability and speed of impact

For a given fragment to be counted as an impact on a house neighboring the source house, its trajectory must travel a specified horizontal distance and fall a certain vertical distance from its original 8.54 m height. Typical across the street distances were measured in Punta Gorda, Florida using Google Earth. It was found that most houses have a distance from the ridge to the

neighboring house across the street in a range of 30 to 60 m. This study considers horizontal distances of 30 m to 60 m in 5 m increments.

Given that a fragment does travel the specified horizontal distance prior to hitting the ground, potential impact on the neighbor is divided into three possibilities based on the vertical position of the fragment: Impact roof (fragment elevation = [6.09 8.54 m]), impact upper story window (fragment elevation = [3.66 5.49 m]), or impact lower story window (fragment elevation = [0.61 2.44 m]).

Fig. 7 illustrates 300 sample trajectories of the 1/8th tile for 44.7 m/s isotach in exposure B. The vertical and horizontal axes represent the vertical and horizontal positions of the fragment after release. Each trajectory was created with a new randomized trace of instantaneous horizontal wind speed. A count of how many trajectories passed through the left face of the house (located 30 m away) at heights corresponding to 1st or 2nd story fenestration or the roof determined the probability of impact. The speed of each trajectory that resulted in impact was collected to determine the average speed of impact. For the Monte Carlo trajectory analysis that follows, 100,000 5 s wind speed traces were generated for each of the eleven isotach values at each of exposures B, C and D.

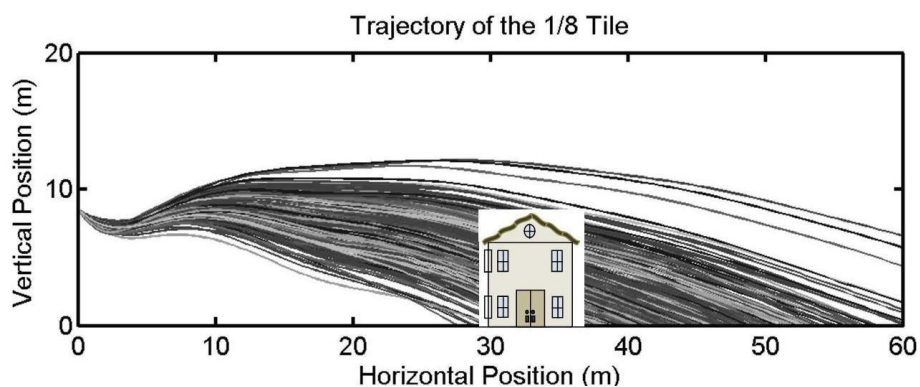


Fig. 7 300 Trajectories of the 1/8th tile for the 100 mph isotach, exposure B

3.3.4 Trajectory model validation

No physical experiments were conducted in the current study to validate the outcomes of the trajectory model. However, the literature provides a means of validation.

The trajectories in Fig. 7 show that the tile fragments fall from their initial height early in the flight, then rise, level off and fall. This increase in height after the initial drop is due to the lift generated by the autorotation of the tile. As the rotational velocity (about the horizontal axis perpendicular to the wind direction) increases, the lift increases and produces the rise in flight. As the tile fragment accelerates in the horizontal plane, the speed differential between the tile and the surrounding wind decreases, which reduces lift and produces the downward trajectory. This behavior has been shown in previously published numerical trajectory studies (e.g., Baker 2007).

This behavior was also observed experimentally in a scale model wind tunnel study of tile and shingle debris trajectories Kordi and Kopp (2011), but was not observed in a study of small plate

flight (Lin *et al.* 2006). The Kordi and Kopp (2011) study also observed that in wind tunnel experiments most debris rotates about all three axes (3D rotation) rather than just the axis horizontal and perpendicular to the wind direction. This rotation about all three axes reduces the lift from autorotation relative to 2D rotation, and reducing flight range. Thus, all other conditions equal, fragments auto-rotating about only the horizontal axis perpendicular to the wind direction (2D model) will travel higher and farther than the fragment rotating about three axes. This overestimate of trajectory range and height is a limitation of the 2D trajectory model which will be revisited during the discussion and interpretation of the results in the next section. The adoption of a 3D trajectory model (e.g., Richards *et al.* 2008) may alleviate this overestimation of trajectory range and height.

The individual impact speeds were collected to determine the average speed of the tile fragment upon impact. The ratio of the average tile fragment impact speed to the expected 3 s gust at roof height was calculated for each isotach wind speed reference, exposure, fragment size, and distance from source to target. This provides a means of validating the trajectory model fragment speed via comparison to experimental findings reported in Kordi and Kopp (2011). In that study it was observed that the in-flight tile velocities span a range of 30–60% of the estimated roof height gust speed. In the current study the range was found to be 40–80%, where the lower values correspond to shorter target distances. The Kordi and Kopp (2011) study utilized whole (intact) roof tiles as debris, whereas the current study modeled 1/8th and 1/4th tile fragments. Smaller, lighter tile fragments will accelerate more quickly than larger, heavier tiles. The ratios of tile fragment speed to gust wind speed in the current study and those found in the Kordi and Kopp (2011) experiments are therefore reasonably consistent. Based on these observations, the discussion of the results will emphasize the speed of impact more so than the probability of impact.

3.3.5 Results of phase 3: trajectory model

Tile fragment trajectories were estimated for 1/8th and 1/4th tile fragments over a range of distances to target, reference wind speed, and reference turbulence. Results are presented in Fig. 8 for the 30 m (left column) and 60 m (right column) flight distances. Each figure contains the mean speed of fragment impact as a function of the 10 m open exposure 3-second reference wind speeds. The top, middle and bottom rows in each figure are results for exposures B, C and D, respectively. Within each plot, results are presented for 6 cases: 1/8th tile fragment impacting the 1st story fenestration, 2nd story fenestration, and roof, and likewise for the 1/4th tile fragment. The horizontal axis is marked with ‘cat 2’, ‘cat 3’, ‘cat 4’, and ‘cat 5’ separated by vertical boundaries. This is in reference to the Saffir-Simpson Hurricane Wind Intensity rating scale, referenced to sustained one minute winds at 10 m in marine exposure. A 1-min marine to 3-second open exposure conversion of 1.1 was applied to provide the boundaries as shown (Simiu *et al.* 2007).

The probability of impact is conditional upon the availability of a single tile fragment at the source location (ridgeline of source house). The probability of this availability and the quantity of such fragments was not determined in this study. In addition, the previous section on validation presented a limitation of the 2D trajectory model regarding the overestimation of the height and distance of the debris flight track. Thus, the impact probabilities are not sufficiently validated to warrant inclusion within the results or conclusions, and the study focuses on the likelihood of puncture given that an impact has occurred.

In Fig. 8 there is no impact speed recorded at several wind speed reference values. This corresponds to no observed impacts at that wind speed. This should not be interpreted literally in light of the above discussion. There is some recourse to interpreting the sparse impact speed plots.

Ultimately the speed of fragment impact is significant with respect to the metal shutter puncture vulnerability data in Fig. 6, which show that a 50% probability of puncture corresponds to an impact speed range of ~ 25 to 35 m/s. Among the exposure C and D impact speed plots in Fig. 8, the lowest impact speeds start at 22.35 m/s for the 44.7 m/s reference wind speed (isotach) and shortest target distance (Fig. 8, middle left). The missing impact speed data at higher isotachs and / or longer target distances will be greater than 22.35 m/s. Thus all of the missing impact speed data will fall within a range that approaches a significant probability of shutter puncture.

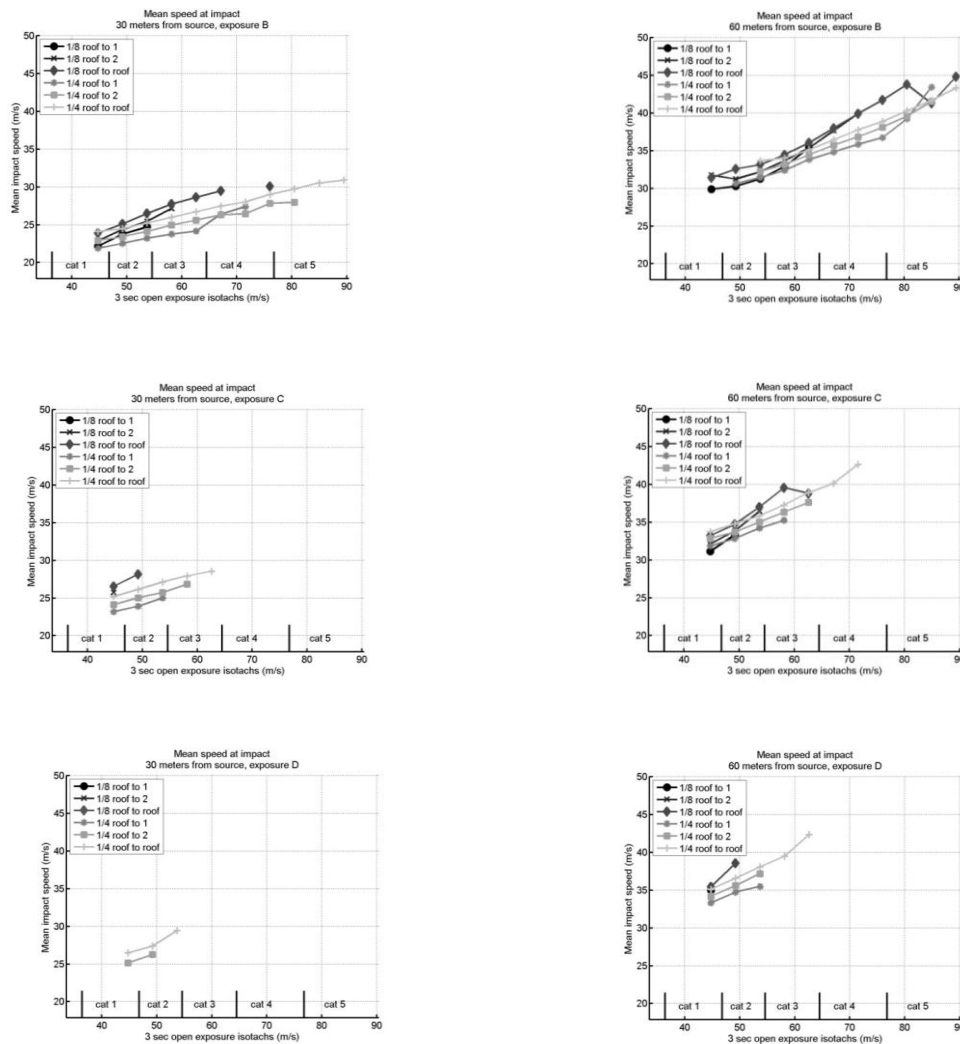


Fig. 8 Mean speed of tile fragment impact for B, C, D exposures, Right column: Distance from source to target = 60 m, Left column: Distance from source to target = 30 m

4. Results interpretation

Interpretation of results is based upon a combined view of puncture probability from phase 2 experimental testing (Fig. 6) and speed of impact (Fig. 8). Recall that the phase 2 experiments were carried out with the fragments impacting point first and perpendicular to the shutter plane. The results in Fig. 6 are thus considered a lower bound for the speed for any given probability of puncture. Consider the circled diamond icon in Fig. 6. The 80% probability of puncture is likely higher than 34 m/s under real conditions. Recall also that each data point in Fig. 6 has a 95% confidence interval of plus or minus 0.2 on the vertical axis. Hence Fig. 6 presents a guideline and not a precise quantification of the impact speed necessary to produce puncture.

Observations:

- Fig. 6 indicates that a significant probability of puncture upon impact occurs for speeds in excess of 30 m/s for 1/8th tile fragments, and in excess of 25 m/s for 1/4th tile fragments. These thresholds are used as benchmarks to draw the forthcoming conclusions of puncture threat with respect to ASCE isotach as well as tropical cyclone intensity.
- In exposure B, 1/8th tile fragment impact speeds exceed 30 m/s at > 76 m/s isotach (Cat 5 winds) for the shortest target distance of 30 m, and > 50 m/s isotach (Cat 2) for the longest target distance of 60 m. This fragment speed threshold of 30 m/s is achieved at lower isotachs for exposure C and D conditions. For the lowest reference wind speed used in this study, 1/8th tile fragments in exposure D are capable of achieving an impact speed with a significant probability of metal shutter puncture.
- In exposure B, 1/4th tile fragment impact speeds exceed 25 m/s at > 60 m/s isotach (mid Cat 3) for the shortest distance of 30 m, and > 44.7 m/s isotach (high Cat 1) for the longest target distance of 60 m. For exposure D, this fragment speed threshold of 25 m/s is reached at the 44.7 m/s isotach for the smallest distance. That is, for the closest distance and lowest reference wind speed used in this study, 1/4th tile fragments in exposure D are capable of achieving an impact speed with a significant probability of metal shutter puncture.

5. Conclusions

The following conclusions are based on the combined results of all three phases of this study:

- Phase 1 (tile frangibility) indicated that the 1/8th tile fragment is the mean size produced from both full and half-size (by weight) tile impact on a tile roof system (Table 1).
- Mechanically attached (single screw) roof systems produce more tile fragments than mortar set roof systems when impacted by a roof tile, all other variables equal (Table 1).
- Given that a tile fragment impact occurs, the likelihood of shutter puncture in winds between 44.7 m/s and 53.6 m/s isotachs (Category 1 and 2 wind events) is small but not insignificant. For exposure C and D conditions and flight distances of > 45 m, fragment impact speeds capable of puncture can be achieved.
- Given that a tile fragment impact occurs, the likelihood of shutter puncture in winds between 58 m/s and 62.5 m/s isotachs (~ Category 3 wind events) is moderate. Minimal impact speed damage threshold can be achieved for short flights in exposures C and D. Impact speeds corresponding to a more significant probability of puncture are achieved for longer flight

distances.

- Given that a tile fragment impact occurs, the likelihood of shutter puncture in winds exceeding the 62.5 m/s isotach (Category 4 or higher) is significant for all exposures and distances in this study. However, the conservative nature of the test protocol (point first perpendicular impact) and trajectory model (use of the highest five second wind trace) renders the achievement of puncture speed a possibility but not necessarily likely.

These conclusions are supported by anecdotal field observations. The authors observed several cases of shutter puncture from tile fragment impact in Punta Gorda, Florida (Charlotte County) caused by Category 4 winds in Hurricane Charley (Fig. 1) in exposure C and D conditions, although the vast majority of metal shutters they observed were not punctured. Shutter puncture was not observed by the authors in regions experiencing less than Category 3 winds from Hurricane Charley or any other sub Category 3 U.S. land falling hurricane since 1999. Lack of direct observation by the authors certainly does not rule out the occurrence of shutter puncture in sub Category 3 tropical cyclones, but to the authors' knowledge no such observation has been reported in damage investigation literature.

The limitations in this study (e.g., 2D trajectory model, debris flight origination from the highest point on a two story roof) and the conservative assumptions employed (e.g., point first impact perpendicular to the shutter, fastest five second segment from each one hour wind simulation) must be considered when interpreting the results. They should be viewed as a conservative guideline rather than an explicit definition of the debris hazard. With this in mind, this study provides supporting evidence that common metal panel window shutters are capable of providing significant protection against a prevalent form of windborne debris in tile roof neighborhoods. However, puncture of metal shutters from roof tile fragments is possible in design level tropical cyclones, and should not be considered a rare or outlier type event.

Acknowledgements

The authors thank the Florida Building Commission for sponsoring this research. The contributions of Mr. Jim Austin and Mr. Scott Bolton are gratefully acknowledged.

References

- ASCE 7-10 (2010), *Minimum design loads for buildings and other structures*, American Society of Civil Engineers, Reston, Virginia.
- Baker, C.J. (2007), "The debris flight equations", *J. Wind Eng. Ind. Aerod.*, **95**, 329-353.
- Beason, W.L. (1974), *Breakage characteristics of window glass subjected to small missile impacts*, Thesis, Civil Engineering Department, Texas Tech University.
- Fernandez, G., Masters, F.J. and Gurley, K.R. (2010), "Performance of hurricane shutters under impact by roof tiles", *Eng. Struct.*, **32**(10), 3384-3393.
- Gurley, K. and Masters, F. (2011), "Post 2004 hurricane field survey of residential building performance", *Nat. Hazard. Rev.*, **12**(4), 177-183.
- Harris, R.I. and Deaves, D.M. (1981), "The structure of strong winds", *Proceedings of the CIRIA Conference on Wind Engineering in the Eighties*, CIRIA, London.
- Holmes, J.D. and Mullins, P.J. (2001), "The mechanics of flying debris and test criteria", *Proceedings of the 5th Asia-Pacific Conference on Wind Engineering*, Kyoto, Japan, October 21-24.

- Holmes, J.D. (2004), "Trajectories of spheres in strong winds with application to windborne debris", *J. Wind Eng. Ind. Aerod.*, **92**, 9-22.
- Holmes, J.D., Letchford, C.W. and Lin, N. (2006), "Investigations of plate-type windborne debris – Part II: computed trajectories", *J. Wind Eng. Ind. Aerod.*, **94**, 21-39.
- Holmes, J.D. (2007), *Wind loading of structures*, 2nd Ed., Taylor & Francis, New York, NY.
- Kordi, B. and Kopp, G.A. (2009a), "Evaluation of quasi-steady theory applied to windborne flat plates in uniform flow", *J. Eng. Mech. - ASCE*, **135**, 657-668.
- Kordi, B. and Kopp, G.A. (2009b), "The debris flight equations by CJ Baker", *J. Wind Eng. Ind. Aerod.*, **97**, 151-154.
- Kordi, B., Traczuk, G. and Kopp, G.A. (2010), "Effects of wind direction on the flight trajectories of roof sheathing panels under high winds", *Wind Struct.*, **13**(2), 145-167.
- Kordi, B. and Kopp, G.A. (2011), "Effects of initial conditions on the flight of windborne plate debris", *J. Wind Eng. Ind. Aerod.*, **99**, 601-614.
- Lin, N., Letchford, C.W. and Holmes, J.D. (2006), "Investigations of plate-type windborne debris. Part I. Experiments in wind tunnel and full scale", *J. Wind Eng. Ind. Aerod.*, **94**(2), 51-76.
- Lin, N. and Vanmarcke, E. (2008), "Windborne debris risk assessment", *Prob. Eng. Mech.*, **23** (4), 523-530.
- Lin, N. and Vanmarcke, E. (2010a), "Windborne debris risk analysis – Part I. Introduction and methodology", *Wind Struct.*, **13**(2), 191-206.
- Lin, N. and Vanmarcke, E. (2010b), "Windborne debris risk analysis – Part II. Application to structural vulnerability modelling", *Wind Struct.*, **13**(2), 207-220.
- Masters, F.J., Gurley, K.R., Shah, N. and Fernandez, G. (2010), "The vulnerability of residential window glass to lightweight windborne debris", *Eng. Struct.*, **32**(4), 911-921.
- Meloy, N., Sen, R., Pai, N. and Mullins, G. (2007), "Roof damage in new homes caused by Hurricane Charley", *J. Perform. Constr. Fac.*, **21**(2), 97-107.
- Minor, J. (1994), "Windborne debris and building envelope", *J. Wind Eng. Ind. Aerod.*, **53**(1-2), 207-227.
- Minor, J. (2005), "Lessons learned from failures of the building envelope in windstorms", *J. Archit. Eng. - ASCE*, **11**(1), 10-13.
- Richards, P.J., Williams, N., Laing, B., McCarty, M. and Pond, M. (2008), "Numerical calculation of the three-dimensional motion of wind-borne debris", *J. Wind Eng. Ind. Aerod.*, **96**, 2188-2202.
- Scarabino, A. and Giacomini, P. (2010), "Analysis of the two dimensional sheet debris flight equations: initial and final state", *Wind Struct.*, **13**(2), 109-125.
- Shinozuka, M. and Deodatis, G. (1991), "Simulation of stochastic processes by spectral representation", *Appl. Mech. Rev.*, **44**(4), 191-204.
- Simiu, E., Vickery, P. and Kareem, A. (2007), "Relation between Saffir-Simpson hurricane scale wind speeds and peak 3-s gust speeds over open terrain", *J. Struct. Eng. - ASCE*, **133**(7), 1043 - 1045.
- Tachikawa, M. (1983), "Trajectories of flat plates in uniform flow with application to wind-generated missiles", *J. Wind Eng. Ind. Aerod.*, **14**, 443-453.
- Tachikawa, M. (1988), "A method for estimating the distribution range of trajectories of wind-borne missiles", *J. Wind Eng. Ind. Aerod.*, **29**(1-3), 175-84.
- Visscher, B.T. and Kopp, G.A. (2007), "Trajectories of roof sheathing panels under high winds", *J. Wind Eng. Ind. Aerod.*, **95**, 697-713.
- Von Karman, T. (1948), "Progress in the statistical theory of turbulence", *P. Natl. Acad. Sci. USA*, **34**, 530-539.
- Wang, K. (2003), *Flying debris behavior*, Thesis, Civil Engineering Department, Texas Tech University.
- Wills, J.A.B., Lee, B.E. and Wyatt, T.A. (2002), "A model of windborne debris damage", *J. Wind Eng. Ind. Aerod.*, **90**(4-5), 555-565.
- Yau Siu, C., Lin, N. and Vanmarcke, E. (2011), "Hurricane damage and loss estimation using an integrated vulnerability model", *Nat. Hazard. Rev.*, **12**(4), 184-189.